JOURNAL OF ENVIRONMENTAL SCIENCES 33 (2015) 106–115

Available online at www.sciencedirect.com

ScienceDirect

www.journals.elsevier.com/journal-of-environmental-sciences

Highly effective removal of Methylene Blue using functionalized attapulgite *via* hydrothermal process

Zhifang Zhang[1,2], *Wenbo Wang*[1,3], *Aiqin Wang*[1,3,*]

1. *Center of Eco-materials and Green Chemistry, Lanzhou Institute of Chemical Physics, Chinese Academy of Sciences, Lanzhou 730000, China. E-mail: zzfwcj@163.com.*
2. *University of the Chinese Academy of Sciences, Beijing 100049, China*
3. *R&D Center of Xuyi Attapulgite Applied Technology, Lanzhou Institute of Chemical Physics, Chinese Academy of Sciences, Xuyi 211700, China*

ARTICLE INFO

Article history:
Received 3 November 2014
Revised 10 December 2014
Accepted 16 December 2014
Available online 10 April 2015

Keywords:
Attapulgite
Hydrothermal
Chloroacetic acid
Methylene Blue
Adsorption

ABSTRACT

Attapulgite (APT) has been frequently used for the adsorptive removal of dyes from aqueous solution owing to its unique one-dimensional nanoscale structure and low-cost, abundant, eco-friendly advantages. In this work, APT was functionalized under mild hydrothermal condition using chloroacetic acid (CA) with –COOH functional groups to improve its adsorption properties. The effect of hydrothermal modification on the microstructure and physicochemical features of APT was investigated by Fourier transform infrared spectroscopy, X-ray diffraction and Field-emission scanning electron microscopy analyses. The effects of hydrothermal reaction parameters on the adsorption properties of modified APT were intensively investigated. It was revealed that the rearrangement of crystal structure and the surface functionalization of APT with –COOH groups cause the surprising increase of adsorption capability for Methylene Blue (MB). The removal ratio of raw APT for MB is only 59.52%, while modified APT could almost completely remove MB in the 200 mg/L of MB solution with a removal ratio of 99.8%. The adsorption kinetics fitted pseudo second-order kinetic model, and the adsorption isotherm could be described with Langmuir isotherm model very well. The hydrogen-bonding interaction, electrostatic attraction and chemical association are the main driving force for the adsorption process.

Introduction

In recent years, environmental contamination problems induced by the excessive discharge of dye and heavy metal pollutants bring severe threat to human health and whole ecosystem, and so the effective elimination of these pollutants from wastewater have aroused worldwide attention. The effluents of dyes drawn a major concern because they are visible, toxic to microorganisms and harmful to human health even at low concentration in wastewater (Verma et al., 2012; Auta and Hameed, 2013; Kabra et al., 2013). Therefore, the removal of dyes from industrial wastewater has been engaged much effort in both academic and industrial fields. During the past decades, many physical, chemical and biological decolorization methods have been used to remove dye; however, some treatment methods are hardly to be accepted by some industries (Ghoreishi and Haghighi, 2003).

Recently, it was found that adsorption is a more efficient method to remove dye than other techniques, and thus it was frequently used to remove different kinds of coloring matter (Qu, 2008; Liu et al., 2010; Wang et al., 2010; Clark and Pitt, 2012). So far, many adsorbents have been widely applied for removing dye. Activated carbon is the most commonly used adsorbent (Hassler,

* *Corresponding authors.* E-mail address: aqwang@licp.cas.cn (Aiqin Wang).

http://dx.doi.org/10.1016/j.jes.2014.12.014

1963). However, it's application in industrial field is still restricted by the expensive cost, and it is still a significant subject to develop a cheaper but effective adsorbent. By contrast, clay minerals have great potential as inexpensive and environmental friendly adsorbents due to their abundance, chemical stability, high surface area and structural properties. The usage of clay minerals or modified clay minerals to remedy dye wastewater presents a soaring interest in recent years (Liu and Zhang, 2007).

Attapulgite (APT, also called as palygorskite) has a larger specific surface area and unique nanoporous structure. Currently, it has attracted widespread attention as a low cost and environmental friendly adsorbent, and has been widely used for the adsorption of various dyes (Giustetto and Wahyudi, 2011; Chen et al., 2011; Liu et al., 2012), heavy metal ions (Potgieter et al., 2006; Chen et al., 2007; Chang et al., 2011) and organic compounds (Al-Futaisi et al., 2007; Guo et al., 2008; Frini-Srasra and Srasra, 2009; Xue et al., 2010) from wastewater. However, these potential applications of APT are highly dependent on the surface properties and active functional groups of APT. Therefore, how to improve the adsorption capacity of natural APT is still a challenge to extend its application. At present, the methods of improving the adsorption performance of APT are mainly focused on acid treatment (Chen et al., 2007; Frini-Srasra and Srasra, 2010), heat treatment (Chen et al., 2006; Su et al., 2012), organification of surface (Frost and Mendelovici, 2006; Zhang et al., 2010), and so on. However, these methods can only enhance the adsorption properties to a limited degree, and the sharp enhancement of the adsorption is hardly to be achieved.

For the past few years, hydrothermal process and functional modification of clay minerals have received attention because it can enhance the performance to a greater degree than conventional techniques. Wu et al. (2013) treated APT by a hydrothermal process and found that the adsorption capacity for Methylene Blue (MB) could be enhanced by 57 mg/g. Li et al. (2014) fabricated a novel montmorillonite supported carbon nanosphere adsorbent (Mt-spC) with glucose as carbon source by a hydrothermal process. Their results showed that the adsorption capacity of the adsorbent for Cr(VI) increased 20 mg/g. Wu et al. (2014) prepared palygorskite/carbon adsorbent through hydrothermal process, which can enhance the absorption capacity for phenol by 74%. These studies confirm hydrothermal process is an extremely effective approach to improve the adsorption property of clay minerals. Therefore, in this study, we modified natural APT using chloroacetic acid (CA) with carboxyl functional groups *via* a hydrothermal process. The functionalized APT was characterized by Fourier transform infrared spectroscopy (FT-IR), X-ray diffraction (XRD) and field-emission scanning electron microscopy (SEM) techniques to investigate the influence of structure change on the properties of APT. Besides, the adsorption properties of functionalized APT for MB were systematically evaluated.

1. Experimental

1.1. Materials

Natural APT is from Huangnishan Mine located at Xuyi County of Jiangsu Province in China, and provided by Huida Mineral Sci-Technology Co. Ltd. (Jiangsu, China). Its chemical compositions are SiO_2 52.37%, Al_2O_3 11.67%, MgO 6.92%, Fe_2O_3 7.91%, CaO 1.91%, K_2O 1.49% and Na_2O 0.27%, as determined by a MiniPal 4 X-ray fluorescence spectrometer (PANalytical Co., Almelo, Netherland). CA ($ClCH_2COOH$, AR grade) was purchased from Sinopharm Chemical Reagent Co., Ltd. (Shanghai, China). MB (indicator grade), with the molecular formula of $C_{16}H_{18}N_3SCl$, was purchased from Alfa Aesar A Johnson Matthey Company, Shanghai, China and used without further purification. All other reagents are of analytical grade and all solution is prepared with deionized water.

1.2. Preparation of functionalized APT

APT was pretreated using 5% of HCl solution at the solid/liquid ratio of 1/10 to remove the associated carbonates. The resultant suspension was passed through a 300-mesh sieve to remove the undesirable quartz. The filtrate was collected and then centrifuged at 5000 r/min for 20 min to separate the solid from the solution. The obtained solid product was fully washed with distilled water until pH around 7. The solid product was oven-dried at 105°C for 4 hr to a constant mass, and then smashed and passed through a 200-mesh screen for further use.

The pretreated APT was uniformly dispersed in 60 mL of aqueous solution of CA at a solid/liquid of 1/200 (M/V) under continuous mechanical stirring. Then, the resultant dispersion was transferred to a 100 mL sealed Teflon reactor, and reacted at 180°C for 48 hr. The reactor was naturally cooled to room temperature, and then the solid was separated by centrifugation at 5000 r/min, and vacuum-dried at 60°C to a constant mass. The raw APT and functionalized APT under hydrothermal condition are marked as RAPT and CA(*x*)-APT (*x* represents the dosage of CA), respectively.

1.3. Adsorption experiment

The adsorption experiments were carried out using the standard batch method as the following procedure: 0.0250 g of APT was added to 25 mL of MB solution (the initial concentration is 200 mg/g), the resultant mixture was fully agitated on a THZ-98A orbital shaker at a fixed speed of 150 r/min and temperature of 30°C for 4 hr to achieve adsorption equilibrium. Afterward, the MB solution was separated from the solid by centrifugation after adsorption process, and used to analyze the residual concentration of MB using a Specord 200UV/Vis spectrophotometer (Hitachi, Japan) at the maximum absorbance wavelength of 665 nm. Then, the amounts of MB adsorbed by per unit mass of adsorbent could be calculated according to the difference of the concentration of MB in solution before and after adsorption (Eq. (1)):

$$q_e = \frac{(C_0 - C) \times V}{W} \quad (1)$$

where, q_e (mg/g) is the adsorption amount of MB; C_0 (mg/L) and C (mg/L) are the concentration of MB solution before and after adsorption, respectively; V (L) is the volume of MB solution used; and W (g) is the mass of the adsorbent used.

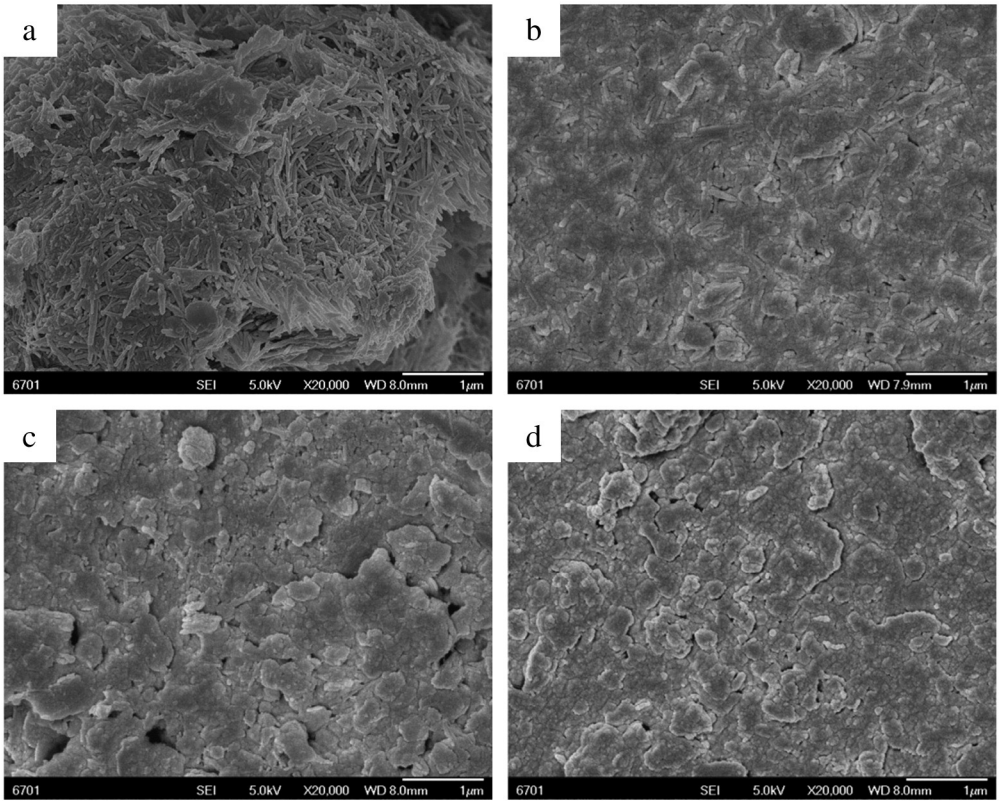

Fig. 1 – Field-emission scanning electron microscopy images of (a) RAPT, (b) CA (0.01)-APT, (c) CA (0.04)-APT, and (d) CA (0.16)-APT.

1.4. *Characterization*

Zeta potential is measured on a ZEN3600 Zeta voltmeter (Malvern, Worcestershire country, Britain). The morphologies are observed using a field-emission scanning electron microscopy (FESEM, JEOL JSM-6701F SEM, Tokyo, Japan). FT-IR spectra are recorded on a Fourier transform infrared spectrometry (Thermo Nicolet NEXUS TM, USA) in the range of 4000–400 cm^{-1} using KBr pellets. Powder XRD patterns are collected using an X-ray diffractometer with Cu anode (PANanalytical Co. X'pert PRO), running at 40 kV and 30 mA. The specific surface area (S_{BET}) is determined by the Brunauer–Emmett–Teller (BET) method. The pore volume (PV) and pore-size (PZ) distribution are estimated by the Barrett–Joyner–Halenda (BJH) method at 77 K (ASAP 2020 V4.00 (V4.00 H), Micromeritics Instrument Corporation).

2. Results and discussion

2.1. *SEM morphologies*

The SEM images of APT before and after functionalized with CA *via* a hydrothermal process are shown in Fig. 1. A lot of bulk crystal bundles composed of rods could be clearly observed in the SEM image of RAPT (Fig. 1a). After modified with different concentration of CA, the crystal bundle of APT was possibly damaged. Only a small amount of nanorods existed and the length of rod becomes shorter. Detailed information can be observed from Fig. 1b–d. As the increase of CA concentration, the surface of APT became more and more rough, in which numerous fine particles were produced and APT embedded in these particles. This may be due to the interaction between CA and APT. Furthermore, it can be clearly observed that a lot of pores were formed on the surface. At the same time, the associated minerals (the amorphous matters in the images) were reduced after hydrothermal process, indicating that the hydrothermal process may decompose the impurity among crystal bundles or aggregates and make them disperse to a better degree.

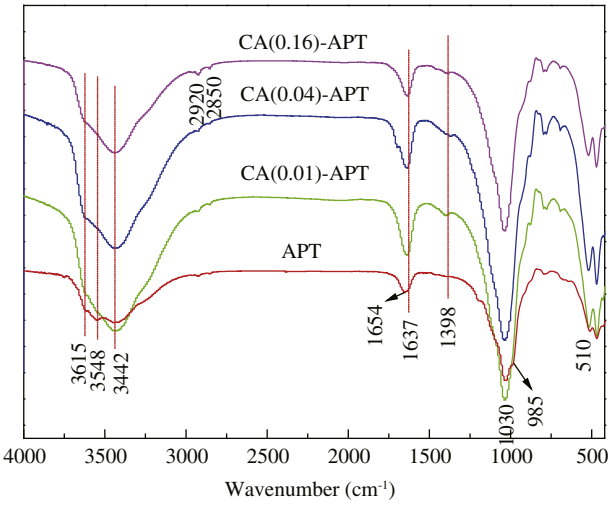

Fig. 2 – FT-IR spectroscopy of RAPT and CA-APT.

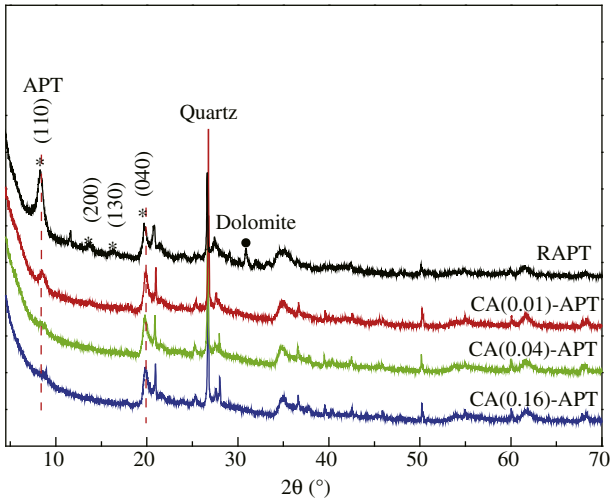

Fig. 3 – X-ray diffraction patterns of RAPT and CA-APT samples.

2.2. FT-IR analysis

The change of chemical structure, especially the surface functional groups of APT after hydrothermal modification can be reflected by the FT-IR analysis. As shown in Fig. 2, the new bands at 2920 cm^{-1} (asymmetric stretching vibration of $-CH_2$), 2850 cm^{-1} (symmetric stretching vibration of $-CH_2$), 1398 cm^{-1} (bending vibration of C–H), and 1734 cm^{-1} (C═O stretching vibration of –COOH) appeared after modification, which give a direct evidence that the CA reacts with APT and bonded on its surface. Meanwhile, several changes could also be observed in the FT-IR spectra of APT: (1) the absorption band of APT at 3580 cm^{-1} (stretching vibration of Al–OH–Fe^{3+}) and 3548 cm^{-1} (the stretching vibration of OH_2 groups) almost disappeared; (2) the absorption band at 1196 cm^{-1}, ascribed to the stretching vibration of Si–O–Si bonds that connect two reverse tetrahedrons (Wu et al., 2011), almost disappeared; (3) the band at 1654 cm^{-1}, attributed to the H–O–H bending vibration modes of the adsorbed, zeolitic and crystal water molecules (Wu et al., 2011), slightly shifts to 1637 cm^{-1}; (4) the bands at 1030 cm^{-1} and 510 cm^{-1}, ascribed to the Si–O–Si stretching vibration and the deformation of tetrahedral sheet, have no obvious change. The band at 1196 cm^{-1} is commonly denoted as the exclusive absorbance band of ribbon-layer silicate, and so its disappearance means the partial damage of the ribbon-layer crystal structure. Comparatively, the SiO_4 tetrahedron was well remained even APT was subject to a hydrothermal process. It could be revealed that some Si–O–Si or Si–O–M bonds may be broken and induced the local collapse or rearrangement of APT crystal. This is fitted with the SEM and XRD results very well.

2.3. XRD analysis

The X-ray diffraction patterns of APT before and after modification further illustrate the structure change of APT. As shown in Fig. 3, the diffraction peaks of (110), (200), (130) and (040) crystal planes of APT appear at 2θ = 8.31°, 13.5°, 16.4° and 19.8°, respectively. After being modified with low dosage of CA (0.01 mol/L), the intensity of these peaks obviously decreased. However, the situation becomes different when the dosage of CA was further increased. The intensity of (110) diffraction peak further decreased (without disappearance), and the (200) and (130) diffraction peaks almost disappeared, indicating that the ribbon-layer structure composed of continuous tetrahedron sheets and discontinuous octahedron sheets deformed and the ordered arrangement of overall lattice structure are partially destroyed (Frost and Ding, 2003). Meanwhile, the diffraction peak at 2θ = 35.1°, corresponding to the tetrahedral sheets, becomes sharper with no obvious change of intensity. It gives direct evidence that the silicon–oxygen tetrahedron chains have not been disintegrated, and the lattice arrangement seems to be more ordered, which is consistent with the FT-IR results (Fig. 2). However, the diffraction peak appearing at 2θ = 19.8° (040) has no change after modification, indicating the octahedral structure of APT does not be damaged. Simultaneously, after hydrothermal treatment, the diffraction peak of dolomite (2θ = 30.9°) diminished and no new diffraction peak was observed. This confirmed that the associated dolomite minerals may be removed during the hydrothermal process.

2.4. BET analysis

The N_2 adsorption–desorption isotherm of APT before and after modified with CA was measured and the textural parameters were calculated by BJH method (Table 1). RAPT presents a high S_{BET} of 226.27 m^2/g with the micropore surface area (S_{micro}) of 68.76 m^2/g and external surface area (S_{ext}) of 157.50 m^2/g. The average pore size (PZ) of RAPT is 6.80 nm, the pore volume (V_{total}) is 0.3846 cm^3/g and the micropore volume (V_{micro}) is 0.0363 cm^3/g. After modified with CA by hydrothermal process, the S_{BET} and PZ decreased with the increase of CA dosage. This is possibly attributed to the reaction between CA and the –OH groups on the surface of APT, which lead to the block of pore or

Table 1 – Microstructural parameters of APT before and after modification.

Samples	S_{BET} (m^2/g)	S_{micro} (m^2/g)	S_{ext} (m^2/g)	V_{total} (cm^3/g)	V_{micro} (cm^3/g)	PZ (nm)
RAPT	226.27	68.76	157.50	0.3846	0.0363	6.80
CA(0.01)-APT	169.32	41.17	128.15	0.2366	0.0219	5.59
CA(0.04)-APT	159.41	39.98	119.43	0.2157	0.0212	5.41
CA(0.16)-APT	159.68	41.08	118.60	0.2110	0.0219	5.29

S_{BET} is the BET specific surface area of APT samples; S_{micro} is the micropore area calculated by the t-Plot method; S_{ext} is the external surface area calculated by the t-Plot method; V_{total} is the total pore volume of pores; V_{micro} is the micropore volume by t-Plot method; and PZ is the average pore width.

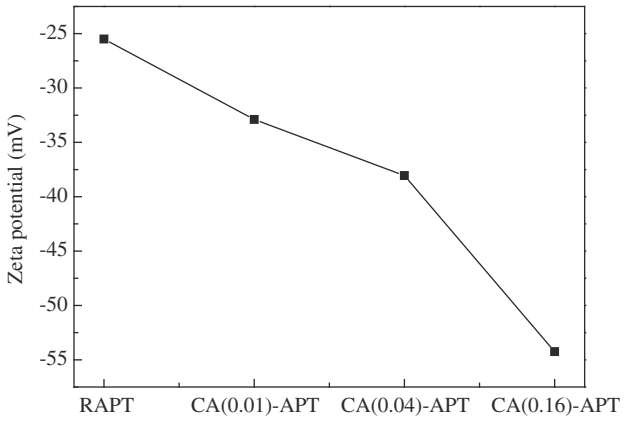

Fig. 4 – Zeta potential of RAPT and CA-APT samples.

tunnel in the crystal. More –COOH is possibly reacted onto APT with the increase of CA dosage, and the specific surface is gradually decreased.

2.5. Zeta potential

The structure change and surface reacting with CA may alter the composition of groups and charge distribution on APT. It can be seen from Fig. 4 that the Zeta potentials of raw and modified APT are all negative, and became more negative after modification. The Zeta potential of raw APT is –25.5 mV, which increases to –32.9, –38.1 and –54.3 mV with increasing the CA concentration to 0.01, 0.04 and 0.16 mol/L, respectively. The main reasons are that, (1) the hydrothermal process causes the breakage of Si–O–Si and Si–O–M bonds and the partial collapse of crystal structure, which may generate more –Si–O^- groups; and (2) the carboxyl groups on the surface of APT bring more negative charge. It was revealed that the functionalization of APT with CA *via* hydrothermal process is more effective to alter the surface groups and charges, because the structure optimization and surface reaction could be achieved by one-step process. The increase of negative charges is favorable to enhance the affinity of APT with cationic matters, *e.g.*, cationic dyes, and then improve the adsorption for them.

2.6. Adsorption capacities

Fig. 5 shows the effect of hydrothermal modification parameters, *e.g.*, CA concentration, pH and solid–liquid ratio on the adsorption capacities of APT for MB. It was observed that the adsorption capacity of APT for MB increased with the increase in CA dosage (Fig. 5a). The adsorption capacity of RAPT for MB is only 119.08 mg/g, whereas it sharply increases to 199.70 mg/g after being modified with 0.04 mol/L of CA solution. With the further increase of CA concentration, the adsorption capacity slightly decreases, indicating that the moderate CA concentration is beneficial to enhance the adsorption removal for MB, and 0.04 mol/L is selected as the optimum concentration. The enhanced adsorption of functionalized APT for MB is mainly ascribed to the contribution of APT and –COOH groups. From Figs. 3 and 4, it can be noticed that the Zeta potential of CA(0.04)-APT is not the most negative, and the structure of APT changes to a greater degree. This may cause the breakage of Si–O–Si and Si–O–M bonds to generate more –Si–O^- groups that are favorable to the adsorption of MB. As the same, the C═O absorbance band of CA(0.04)-APT is more obvious than the others, implying that more –COOH groups were attached on the surface of APT, which may contribute to the enhancement of adsorption capacity.

Fig. 5b shows the effects of pH on the adsorption capacity of APT for MB. It is obvious that the adsorption capacity increased with increasing pH values and reached the maximum at pH 5. As discussed above, the structure and surface groups of APT could be changed after hydrothermal modification. At acidic condition, the Si–OH groups on APT are existed as the protonation state Si–OH_2^+, which has weaker affinity with cationic MB. When pH increased to above 5, the Si–OH may react with CA more easily, and such a range of pH is favorable to the reaction of –COOH groups, which is helpful to the adsorption of MB. Thus, pH 5 was identified as the optimum condition.

Fig. 5c shows the effect of solid/liquid ratio on the adsorption capacities of modified APT for MB. It is clearly observed that the adsorption capacity of APT was greatly increased from 119.08 mg/g (for RAPT) to 199.70 mg/g (for CA-APT) after being modified at the solid/liquid ratio of 1/200. It is encouraging that the optimal sample can almost completely remove the MB in the solution with the initial concentration of 200 mg/g, which indicates that the functionalized APT can be used as a high-efficient adsorbent for the removal of cationic dyes.

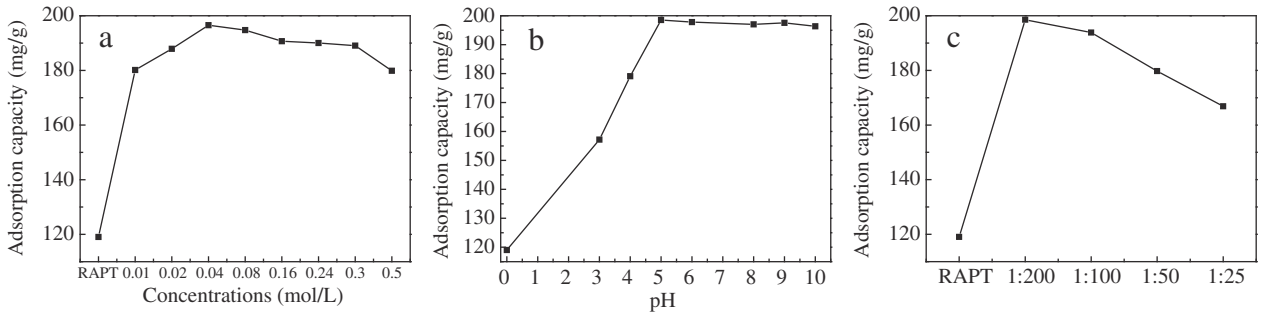

Fig. 5 – Effect of concentration of CA (a), pH of CA solution (b), solid–liquid ratio (c) on the adsorption properties of APT for MB.

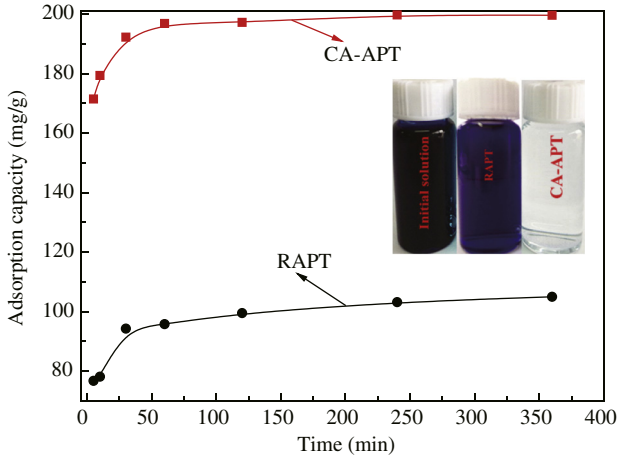

Fig. 6 – Effect of contact time on adsorption of RAPT and CA-APT for MB.

2.7. Effect of contact time on adsorption

As an adsorbent, adsorption rate is especially important to its practical application. Fig. 6 shows the effect of contact time on the adsorption properties of APT. As can be seen, the adsorption rate of functionalized APT is very fast and the adsorption equilibrium could be reached within 60 min, indicating that the adsorption of APT for MB is a rapid process. Also, removal ratio of functionalized APT for MB is evidently higher than that of RAPT, and 99.8% of MB could be removed. The MB solution with the initial concentration of 200 mg/L could be decolored by CA-APT, but the color is still deep-blue after adsorbed with RAPT (the inset in Fig. 6). In order to study the adsorption kinetics of APT for MB, the commonly used kinetic models, including the pseudo first-order (Eq. (2)) (Lagergren, 1898; Ho, 2004) and pseudo second-order (Eq. (3)) (Ho and Mckay, 1999a, 1999b, 2000) kinetic models, were introduced:

$$\ln(q_e - q_t) = \ln q_e - k_1 t \quad (2)$$

$$\frac{t}{q_t} = \frac{1}{k_2 q_e^2} + \frac{t}{q_e} \quad (3)$$

where, q_e (mg/g) is the amount of dye adsorbed at equilibrium; q_t (mg/g) is the amount of dye adsorbed by per unit mass of adsorbent at any time t (sec); k_1 (min^{-1}) and k_2 (g/(mg·min)) are the rate constants calculated from pseudo first-order and pseudo second-order kinetic models, respectively. As shown in Fig. 7, the linear correlation coefficient ($R^2 < 0.9317$) obtained from the fitting data by pseudo first-order kinetic model is very low; whereas the fitting curves from pseudo second-order model present straight lines with higher correlation coefficient ($R^2 > 0.9998$). Also, the theoretically calculated q_{2e} from pseudo second-order model is almost equivalent to the experimental data, but the obtained q_{1e} value from pseudo first-order model has obvious difference from the experimental data (Table 2). Therefore, the pseudo second-order kinetic model is more suitable to describe the adsorption behaviors of APT and CA-APT for MB, which means that the adsorption process is inclined to an associated chemisorption and surface diffusion process, and the electrostatic and interior complexing interaction provide the main driving force for adsorption.

2.8. Effect of initial concentration and adsorption isotherms

It is crucial that how the adsorbed molecules divide themselves into the liquid phase and solid phase until the adsorption process attains an equilibrium state. The effect of initial MB concentration on the adsorption capacities of APT samples is shown in Fig. 8. It can be seen that the adsorption capacities quickly increased with the increase of initial concentration, and achieve equilibrium at the concentration higher than 200 mg/L, which means that almost all of the available adsorption sites on the APT samples may be saturated at the equilibrium state (Fig. 8a). In order to illustrate the adsorption process and mechanism, the Langmuir and Freundlich isotherm models were adopted to analyze the experimental data, and the results are shown in Fig. 8b–d. The linear forms of Langmuir and Freundlich equations are presented as follows (Langmuir, 1918; Ho et al., 2002):

$$\frac{c_e}{q_e} = \frac{1}{b \times q_m} + \frac{c_e}{q_m} \quad (4)$$

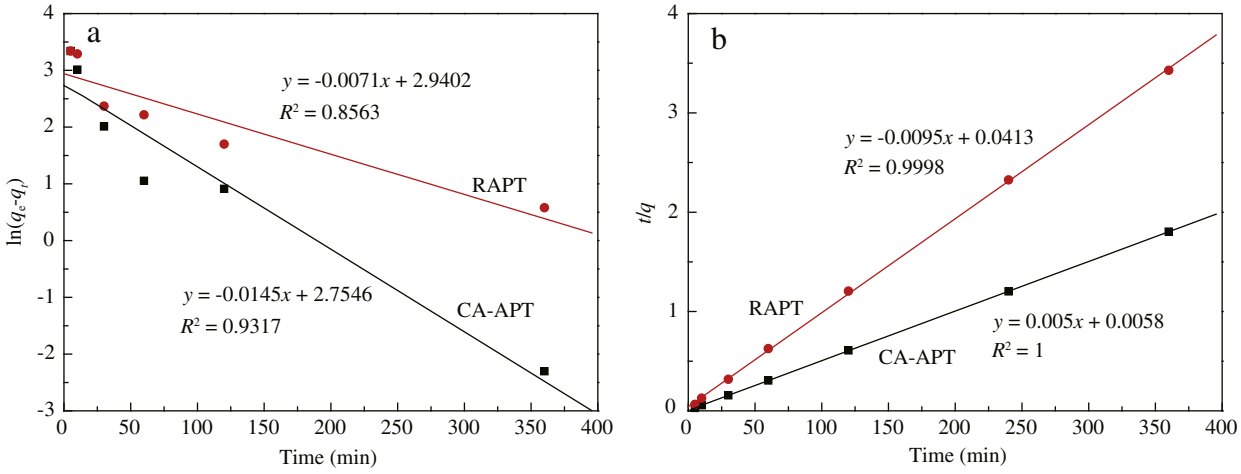

Fig. 7 – Adsorption kinetic curve fitted by pseudo first-order model (a) and pseudo second-order model (b).

Table 2 – Adsorption kinetic parameters of RAPT and CA-APT for MB.

Samples	q_{exp} (mg/g)	Pseudo first-order model			Pseudo second-order model		
		$q_{1e\backslash}$ (mg/g)	$k_1 \times 10^3$ (min^{-1})	R^2	q_{2e} (mg/g)	$k_2 \times 10^3$ (g/(mg min))	R^2
RAPT	105.01	18.92	7.1	0.8563	105.26	2.19	0.9998
CA-APT	199.70	15.71	14.5	0.9317	200.00	4.31	1

$$\log q_e = \log K_F + \frac{1}{n}\log c_e \quad (5)$$

where, q_m (mg/g) is the saturated adsorption capacity calculated from Langmuir fitted lines, C_e (mg/L) and q_e (mg/g) are the concentration of MB after adsorption and the equilibrium adsorption capacity, respectively. The constant b (L/mg) is in relation to the adsorption energy. K_F ((mg/g)(L/mg)$^{1/n}$) is a Freundlich constant and roughly defined as the adsorption capacity. The constant $1/n$ usually represents the adsorption intensity.

The dimensionless equilibrium parameter (R_L) is the significant characteristic of Langmuir isotherm, which can be expressed by the following equation (Hall et al., 1966):

$$R_L = \frac{1}{1 + b \times c_0} \quad (6)$$

where, b is the constant as in the Langmuir isotherm equation (Eq. (4)). C_0 (mg/L) is the initial concentration of MB solution. The R_L value is calculated from the Eq. (6) by fitting the plot of R_L *vs* C_0, which reflects the shape of isotherm. If $R_L > 1$, it is unfavorable for adsorption; while $0 < R_L < 1$ suggests a favorable adsorption; $R_L = 1$ indicates that the plot is linear, belonging to linear adsorption; $R_L = 0$ implies it is irreversible.

The equilibrium adsorption data was fitted by the Langmuir and Freundlich isotherm models (Fig. 8c and d), and the parameters and linear correlation coefficients calculated from the slope and intercept of fitting plots are listed in Table 3. As can be seen, the linear correlation coefficient (R^2 = 0.9999) calculated from the Langmuir isotherm model is better than those calculated from Freundlich isotherm model (R^2 = 0.6553). In addition, the experimental adsorption

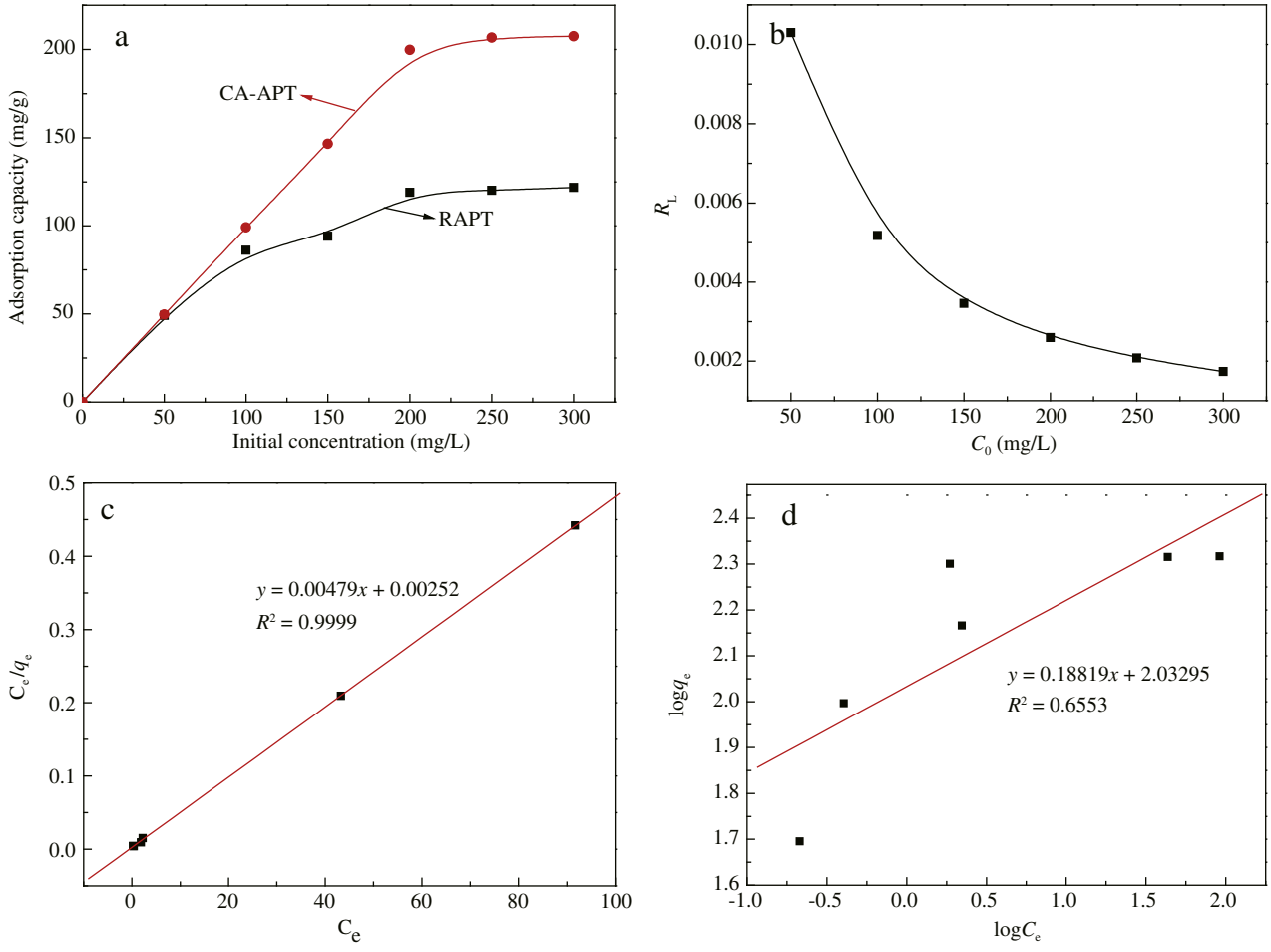

Fig. 8 – Effect of initial concentration on the adsorption of CA-APT for MB (a), (b) plot of the R_L values for MB adsorption at different initial concentrations, Langmuir (c) and Freundlich isotherm model (d) fitting curves for the adsorption of MB on CA-APT.

Table 3 – Isotherm parameters for the adsorption of MB onto the CA-APT.

Samples	Langmuir model				Freundlich model		
	q_e (mg/g)	q_m (mg/g)	b (L/mg)	R^2	n	K_F	R^2
CA-APT	207.48	208.33	1.92	0.9999	5.31	107.87	0.6553

capacity (q_e = 207.48 mg/g) is very close to the theoretical value (208.33 mg/g), which revealed that the adsorption process was supposed to obey the Langmuir model, instead of the Freundlich model. Langmuir isotherm is used to the assumption that all of the adsorption sites are identical on the adsorbent. So, the fitting results suggest that the monolayer adsorption only occurs on a surface, instead of immigration of adsorbate on the surface (Langmuir, 1918). Furthermore, the curves of R_L *versus* initial MB concentration are presented in Fig. 8b. It can be seen that the values of R_L are in the range of 0.002–0.010, in the range of 0–1, which indicate that it is favorable to adsorption and close to the ideal irreversible case (Gupta et al., 2006).

Fig. 9 presented the removal ratio of RAPT and CA-APT for MB (initial concentration, 200 mg/L). The removal ratio of CA-APT for MB (99.8%) is much higher than that of RAPT (59.52%). This means that the CA-APT may almost completely remove the MB in 200 mg/L of solution, and is valuable to the practical application. Table 4 compared adsorption capacity of CA-APT for MB with various kinds of previously reported adsorbents, such as MMT@C nanocomposites (Ai and Li, 2013), attapulgite/bentonite (50%) (Liu et al., 2014), titanate nanotubes (Xiong et al., 2010), grinding palygorskite (Guo et al., 2008), powdered activated carbon (Yener et al., 2008), MtMIO material (Cottet et al., 2014), sepiolite (Auta and Hameed, 2012), and palygorskite (Frini-Srasra and Srasra, 2009). It could be clearly observed that the functionalized CA-APT adsorbent shows a relatively higher adsorption capacity for MB than the others.

The FT-IR spectra of the adsorbent before and after adsorption were measured to study the adsorption mechanism, and the results are shown in Fig. 10. As shown in Fig. 10b, the absorption band of hydroxyl groups at about 1654 cm^{-1} for APT-MB slightly weakened, but it almost disappear for APT-CA-MB materials. The above results indicate that hydrogen-bonding interaction generated between APT and MB, and then the adsorption capability was enhanced. Compared with the FT-IR spectra of samples before adsorbing MB (Fig. 1), after adsorbing MB, the new absorption bands at about 1601 cm^{-1}, 1396 cm^{-1} and 1352 cm^{-1} were observed. These peaks belong to the stretching vibration of the C═S and C – N bond of MB (Xiong et al., 2010; Ai et al., 2011; Ma et al., 2012). All the absorption peaks for CA-APT-MB is stronger than those of APT-MB, indicating the MB could be joined tightly on the surface of CA-APT adsorbent during the adsorption process. Besides, the weak absorption peak at about 1734 cm^{-1} (ascribed to the –COOH bending vibration in CA-APT) is possibly overlapped with the peak of MB. This further suggests the strong interaction between CA-APT and MB molecules. In addition, the modified APT obtained by hydrothermal process at low concentration of CA solution is also negatively charged due to the presence of oxygen-containing groups. Compared to the raw APT, the surface charges of modified APT are more negative as shown by the Zeta potential results. Then it is regarded that the electrostatic interaction occurs between negatively charged modified APT and positively charged MB molecules, which resulting in the surprising adsorption of CA-APT for MB. Meanwhile, the hydrogen-bonding interaction would generate between the Si–OH groups of APT and MB, but for modified APT, which is more intensive than that of RAPT. As illustrated in Fig. 10a, the additionally generated strong electrostatic attraction and the chemical association between –COOH groups of CA-APT and MB molecules may be responsible for the hither adsorption removal capacity of CA-APT for MB.

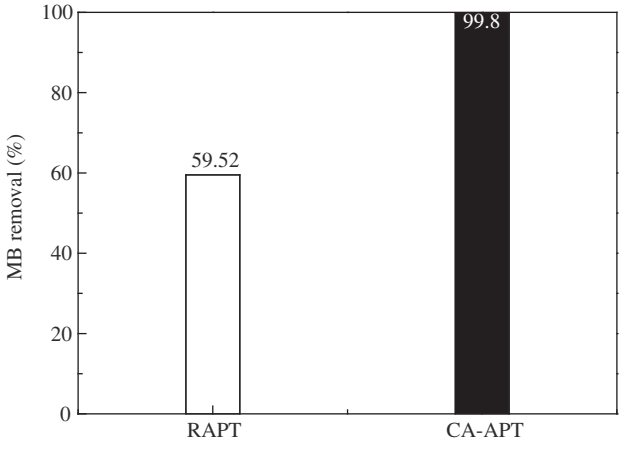

Fig. 9 – Comparative adsorption removal of RAPT and CA-APT towards Methylene Blue.

3. Conclusions

A functionalized CA-APT adsorbent was fabricated by a facile one-step hydrothermal process using CA as the modifier. The inert Si–O–Si and Si–O–M bonds in the crystal backbone

Table 4 – Comparison of the adsorption capacities of MB onto various adsorbents.

Adsorbents	q_m (mg/g)	References
CA-APT	207.48 [a]	In this work
MMT@C nanocomposites	194.2	Ai and Li (2013)
Attapulgite/bentonite (50%)	168.63	Liu et al. (2014)
Titanate nanotubes	133.33	Xiong et al. (2010)
Grinding palygorskite	111.78	Liu et al. (2012)
Powdered activated carbon	91	Yener et al. (2008)
MtMIO	69.11	Cottet et al. (2014)
Sepiolite	57.38	Auta and Hameed (2012)
Palygorskyte	48.39	Chen et al. (2011)
Porous MnO_2 microspheres	259.2 (80°C)	Chen et al. (2013)
BAU-CL	33.65	Kadirova et al. (2013)

[a] Initial MB concentration, 300 mg/g; adsorbent dosage, 1 g/L.

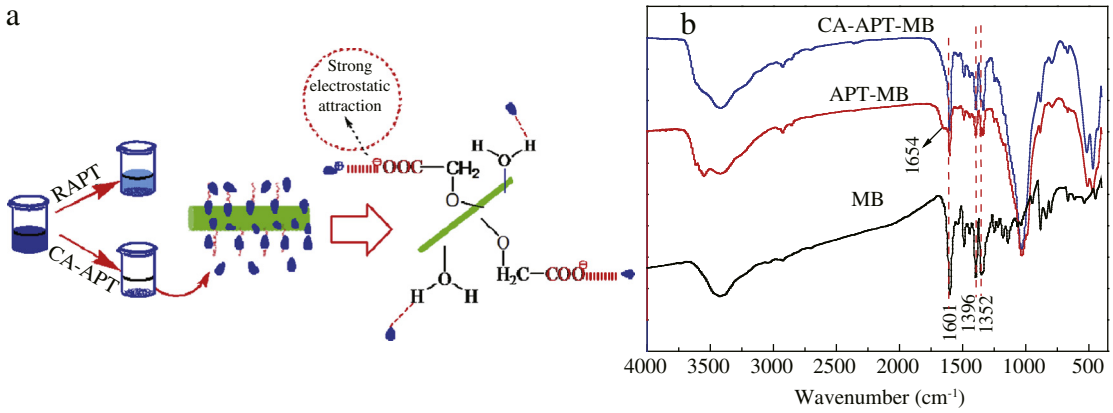

Fig. 10 – (a) Mechanism illustration of the adsorption process and interaction between CA-APT and MB (indicated by blue points); (b) FT-IR spectroscopy of MB, MB-loaded APT and MB-loaded CA-APT.

of APT could be broken during hydrothermal process, and more active sites generated on the APT. CA reacted with APT, and bring – COOH groups on its surface to form more adsorption sites. The adsorption properties of the functionalized APT for MB were systematically evaluated by batch adsorption experiments. It was found that the resultant functionalized APT shows surprisingly better adsorption performance. The adsorption capacity of raw APT for MB is only 119.08 mg/g, but it sharply increased to 199.70 mg/g (enhanced by 67.8%). More importantly, the raw APT can only remove 59.5% of MB from 200 mg/L of initial solution, while the functionalized APT can almost thoroughly remove the MB in the same concentration, with a removal rate of 99.8%. The adsorption of modified APT for MB follows the pseudo second-order kinetic model and the Langmuir isotherm very well, suggesting that both the physical and chemical adsorption process contributes to the adsorption process. The adsorption process is involved with the synergistic effect of hydrogen-bonding interaction, electrostatic attraction and chemisorptions. Therefore, the functionalized APT adsorbents derived from abundant, low-cost, non-toxic and stable APT minerals show excellent adsorption capacity and higher removal rate for MB, which are a promising candidate for the application in the fields of environment remedy.

Acknowledgments

This work was supported by the Hi-Tech research and Development Program (863) of China (No. 2013AA032003) and the West Light Foundation of the Chinese Academy of Sciences (the Science Development Talent Teach words [2012] No. 179).

REFERENCES

Ai, L.H., Li, L.L., 2013. Efficient removal of organic dyes from aqueous solution with ecofriendly biomass-derived carbon@ montmorillonite nanocomposites by one-step hydrothermal process. Chem. Eng. J. 223, 688–695.

Ai, L.H., Zhang, C.Y., Liao, F., Wang, Y., Li, M., Meng, L.Y., et al., 2011. Removal of methylene blue from aqueous solution with magnetite loaded multi-wall carbon nanotube: kinetic, isotherm and mechanism analysis. J. Hazard. Mater. 198, 282–290.

Al-Futaisi, A., Jamrah, A., Al-Hanai, R., 2007. Aspects of cationic dye molecule adsorption to palygorskite. Desalination 214 (1), 327–342.

Auta, M., Hameed, B.H., 2012. Modified mesoporous clay adsorbent for adsorption isotherm and kinetics of methylene blue. Chem. Eng. J. 198–199, 219–227.

Auta, M., Hameed, B.H., 2013. Acid modified local clay beads as effective low-cost adsorbent for dynamic adsorption of methylene blue. J. Ind. Eng. Chem. 19 (4), 1153–1161.

Chang, Y., Liu, H.W., Zha, F., Chen, H.K., Ren, X.N., Lei, Z.Q., 2011. Adsorption of Pb(II) by N-methylimidazole modified palygorskite. Chem. Eng. J. 167 (1), 183–189.

Chen, T.H., Wang, J., Qin, C.S., Peng, S.C., Song, Y.X., Guo, Y., 2006. Effect of heat treatment on structure, morphology and surface properties of palygorskite. J. Chin. Ceram. Soc. 34 (11), 1406–1410.

Chen, H., Zhao, Y.G., Wang, A.Q., 2007. Removal of Cu(II) from aqueous solution by adsorption onto acid-activated palygorskite. J. Hazard. Mater. 149 (2), 346–354.

Chen, H., Zhao, J., Zhong, A.G., Jin, Y.X., 2011. Removal capacity and adsorption mechanism of heat-treated palygorskite clay for methylene blue. Chem. Eng. J. 174 (1), 143–150.

Chen, R.X., Yu, J.G., Xiao, W., 2013. Hierarchically porous MnO_2 microspheres with enhanced adsorption performance. J. Mater. Chem. A 1 (38), 11682–11690.

Clark, S.E., Pitt, R., 2012. Targeting treatment technologies to address specific stormwater pollutants and numeric discharge limits. Water Res. 46 (20), 6715–6730.

Cottet, L., Almeida, C.A.P., Naidek, N., Viante, M.F., Lopes, M.C., Debacher, N.A., 2014. Adsorption characteristics of montmorillonite clay modified with iron oxide with respect to methylene blue in aqueous media. Appl. Clay Sci. 95 (1), 25–31.

Frini-Srasra, N., Srasra, E., 2009. Adsorption of quinalizarin from non aqueous solution onto acid activated palygorskite. Surf. Eng. Appl. Electrochem. 45 (4), 306–311.

Frini-Srasra, N., Srasra, E., 2010. Acid treatment of south Tunisian palygorskite: removal of Cd (II) from aqueous and phosphoric acid solution. Desalination 250 (1), 26–34.

Frost, R.L., Ding, Z., 2003. Controlled rate thermal analysis and differential scanning calorimetry of sepiolites and palygorskites. Thermochim. Acta 397 (1-2), 119–128.

Frost, R.L., Mendelovici, E., 2006. Modification of fibrous silicates surfaces with organic derivatives: an infrared spectroscopic study. J. Colloid Interface Sci. 294 (1), 47–52.

Ghoreishi, S.M., Haghighi, R., 2003. Chemical catalytic reaction and biological oxidation for treatment of non-biodegradable textile effluent. Chem. Eng. J. 95 (1-3), 163–169.

Giustetto, R., Wahyudi, O., 2011. Sorption of red dyes on palygorskite: synthesis and stability of red/purple mayan

nanocomposites. Microporous Mesoporous Mater. 142 (1), 221–235.
Guo, X.L., Yao, Y.D., Yin, G.F., Kang, Y.Q., Luo, Y., Zhuo, L., 2008. Preparation of decolorizing ceramsites for printing and dyeing wastewater with acid and base treated clay. Appl. Clay Sci. 40 (1-4), 20–26.
Gupta, V.K., Mohan, D., Saini, V.K., 2006. Studies on the interaction of some azo dyes (naphthol red-J and direct orange) with nontronite mineral. J. Colloid Interface Sci. 298 (1), 79–86.
Hall, K.R., Eagleton, L.C., Acrivos, A., Vermeulen, T., 1966. Pore and solid-diffusion kinetics in fixed-bed adsorption under constant pattern conditions. Ind. Eng. Chem. Res. Fundam. 5 (2), 212–223.
Hassler, J.W., 1963. Activated Carbon. Chemical Publication, New York.
Ho, Y.S., 2004. Citation review of Lagergren kinetic rate equation on adsorption reactions. Scientometrics 59 (1), 171–177.
Ho, Y.S., Mckay, G., 1999a. Pseudo-second order model for sorption processes. Process Biochem. 34 (5), 451–465.
Ho, Y.S., Mckay, G., 1999b. Comparative sorption kinetic studies of dyes and aromatic compounds onto fly ash. J. Environ. Sci. Health Part A Toxic/Hazard. Subst. Environ. Eng. 34 (5), 1179–1204.
Ho, Y.S., Mckay, G., 2000. The kinetics of sorption of divalent metal ions onto sphagnum moss peat. Water Res. 34 (3), 735–742.
Ho, Y.S., Huang, C.T., Huang, H.W., 2002. Equilibrium sorption isotherm for metal ions on tree fern. Process Biochem. 37 (12), 1421–1430.
Kabra, A.N., Khandare, R.V., Govindwar, S.P., 2013. Development of a bioreactor for remediation of textile effluent and dye mixture: a plant–bacterial synergistic strategy. Water Res. 47 (3), 1035–1048.
Kadirova, Z.C., Katsumata, K., Isobe, T., Matsushita, N., Nakajima, A., Okada, K., 2013. Adsorption and photodegradation of methylene blue by iron oxide impregnated on granular activated carbons in an oxalate solution. Appl. Surf. Sci. 284, 72–79.
Lagergren, S., 1898. About the theory of so-called adsorption of soluble substance. Kung. Sven. Veten. Hand. 24 (4), 1–39.
Langmuir, I., 1918. The adsorption of gases on plane surfaces of glass, mica and platinum. J. Am. Chem. Soc. 40 (9), 1361–1403.
Li, T., Shen, J.F., Huang, S.T., Li, N., Ye, M.X., 2014. Hydrothermal carbonization synthesis of a novel montmorillonite supported carbon nanosphere adsorbent for removal of Cr(VI) from waste water. Appl. Clay Sci. 93–94, 48–55.
Liu, P., Zhang, L., 2007. Adsorption of dyes from aqueous solutions or suspensions with clay nano-adsorbents. Sep. Purif. Technol. 58 (1), 32–39.
Liu, Y., Zheng, Y.A., Wang, A.Q., 2010. Enhanced adsorption of methylene blue from aqueous solution by chitosan-g-poly (acrylic acid)/vermiculite hydrogel composites. J. Environ. Sci. 22 (4), 486–493.
Liu, Y., Wang, W.B., Wang, A.Q., 2012. Effect of dry grinding on the microstructure of palygorskite and adsorption efficiency for methylene blue. Powder Technol. 225, 124–129.
Liu, Y., Kang, Y.R., Mu, B., Wang, A.Q., 2014. Attapulgite/bentonite interactions for methylene blue adsorption characteristics from aqueous solution. Chem. Eng. J. 237, 403–410.
Ma, J., Yu, F., Zhou, L., Jin, L., Yang, M.X., Luan, J.S., et al., 2012. Enhanced adsorptive removal of methyl orange and methylene blue from aqueous solution by alkali-activated multiwalled carbon nanotubes. Appl. Mater. Interfaces 4 (11), 5749–5760.
Potgieter, J.H., Potgieter-Vermaak, S.S., Kalibantonga, P.D., 2006. Heavy metals removal from solution by palygorskite clay. Miner. Eng. 19 (5), 463–470.
Qu, J.H., 2008. Research progress of novel adsorption processes in water purification: a review. J. Environ. Sci. 20 (1), 1–13.
Su, D.H., Wang, C.H., Cai, S.M., Mu, C.D., Li, D.F., Lin, W., 2012. Influence of palygorskite on the structure and thermal stability of collagen. Appl. Clay Sci. 62–63, 41–46.
Verma, A.K., Dash, R.R., Brunia, P., 2012. A review on chemical coagulation/flocculation technologies for removal of colour from textile wastewaters. J. Environ. Manag. 93 (1), 154–168.
Wang, Y.S., Zeng, L., Ren, X.F., Song, H., Wang, A.Q., 2010. Removal of methyl violet from aqueous solutions using poly (acrylic acid-co-acrylamide)/attapulgite composite. J. Environ. Sci. 22 (1), 7–14.
Wu, X.P., Zhu, W.Y., Zhang, X.L., Chen, T.H., Frost, R.L., 2011. Catalytic deposition of nanocarbon onto palygorskite and its adsorption of phenol. Appl. Clay Sci. 52 (4), 400–406.
Wu, X.P., Liu, C., Zhang, L., Zhang, X.L., Cheng, L.P., 2013. Effect of hydrothermal treatment on structural character of palygorskite and adsorption efficiency for methylene blue. Adv. Mater. Res. 726–731, 560–564.
Wu, X.P., Gao, P., Zhang, X.L., Jin, G.P., Xu, Y.Q., Wu, Y.C., 2014. Synthesis of clay/carbon adsorbent through hydrothermal carbonization of cellulose on palygorskite. Appl. Clay Sci. 95, 60–66.
Xiong, L., Yang, Y., Mai, J.X., Sun, W.L., Zhang, C.Y., Wei, D.P., et al., 2010. Adsorption behavior of methylene blue onto titanate nanotubes. Chem. Eng. J. 156 (2), 313–320.
Xue, A.L., Zhou, S.Y., Zhao, Y.L., Lu, X.P., Han, P.F., 2010. Adsorption of reactive dyes from aqueous solution by silylated palygorskite. Appl. Clay Sci. 48 (4), 638–640.
Yener, J., Kopac, T., Dogu, G., Dogu, T., 2008. Dynamic analysis of sorption of methylene blue dye on granular and powdered activated carbon. Chem. Eng. J. 144 (3), 400–406.
Zhang, L.X., Jin, Q.Z., Huang, J.H., Liu, Y.F., Shan, L., Wang, X.G., 2010. Modification of palygorskite surface by organofunctionalization for application in immobilization of $H_3PW_{12}O_{40}$. Appl. Surf. Sci. 256 (20), 5911–5917.